PHYSICAL REVIEW D VOLUME 40, NUMBER 9 1 NOVEMBER 1989

Next-to-leading-logarithm calculation of jet photoproduction

H. Baer, J. Ohnemus, and J. F. Owens
Department of Physics, Florida State University, Tallahassee, Florida 32306
(Received 26 May 1989)

A Monte Carlo program containing both leading-logarithm and next-to-leading-logarithm contributions has been developed and used to study the photoproduction of large-transverse-momentum hadronic jets. Predictions are presented and discussed for a variety of observables including single-jet invariant cross sections, dijet cross sections, and angular distributions. For some observables the inclusion of the next-to-leading-logarithm terms dramatically lessens the dependency on the choice of the renormalization and factorization scales entering the calculation, thereby increasing the precision of the calculation. The flexibility of the Monte Carlo technique allows predictions for additional observables to be generated easily.

I. INTRODUCTION

Much of our knowledge concerning parton distributions and the dynamics of the underlying parton-parton interactions has been obtained via the use of processes involving photons in the initial or final states or both. The advantages of an electromagnetic probe for studying hadronic constituents are numerous and well known. Briefly, one is using a well-understood interaction in order to obtain information on unknown constituent distributions or interactions. The pointlike nature of the coupling between photons and charged particles allows one to have a greater degree of control over the kinematics of the process under study than if purely hadronic processes were to be used. The event structure of processes containing photons is often cleaner since the photon is replacing a hadronic jet in the final state or an incoming hadron in the initial state.

The results presented in this paper are for processes involving the photoproduction of jets. As discussed in Ref. 1, this reaction possesses a number of distinct advantages for studying parton-parton interactions. The use of a photon beam leads to a cleaner event structure than for the hadron case because, in a large fraction of the high-p_T events, there is no beam jet; the photon interacts in a pointlike manner depositing its full energy into the subprocess. The absence of the beam jet leads to a cleaner final state while the larger fraction of beam energy available for hard scattering means there is an increased efficiency for jet production at large values of momentum transfer. In addition, the detection of jets in the final state allows one to reconstruct the kinematics of the process at the parton level. In the usual leading-logarithm formulation of two-body scattering this process only involves one parton distribution function corresponding to the target. The photon and the two final-state jets allow three of the four participating four-vectors to be measured. Such control over the interacting particles makes this process extremely useful for observing hard scattering at the parton level. The leading-logarithm calculation of the pointlike component involves only two subprocesses: $\gamma q \to gq$ and $\gamma g \to q\bar{q}$, which shall be referred to as the Compton and annihilation subprocesses, respectively.[2] These subprocesses have an angular distribution which is distinctly different from the t-channel processes which dominate jet production with hadronic beams.

In addition to this class of events, there are events which involve the structure function of the photon.[1] That is, some fraction of the time the photon interacts as a hadron, with appropriate quark and gluon distributions.[3] These can be calculated to leading-logarithmic accuracy using, for example, the appropriate Altarelli-Parisi equations.[1,4] The quark distributions in a photon can be measured in two-photon events at an e^+e^- collider, in complete analogy with measuring structure functions in deep-inelastic lepton scattering from a nucleon target. A recent review of the experimental measurements of the photon structure function and a comparison with the theoretical predictions can be found in Ref. 5. By comparing the pointlike and structure-function events in high-p_T jet photoproduction, it will be possible to ascertain the role of the photon quark and gluon distributions. Notice that by performing this separation, one obtains the same type of information as from a hadron beam experiment (qq, qg, and gg scattering subprocesses) in addition to the new information provided by the pointlike terms (Compton and annihilation subprocesses). The utility of this separation has recently been emphasized for forthcoming DESY HERA experiments.[6,7] In addition, an experiment currently under construction at Fermilab, E-683, should have the capability of measuring observables similar to those discussed herein.

The leading-logarithm approximation lies at the heart of most hard-scattering calculations. By now, it is widely recognized that one of the weak points in such a calculation is that one has only an order-of-magnitude estimate for the renormalization and factorization scales. Typically, these are expected to be of the order of the square of the hard-scattering momentum transfer, e.g., p_T^2 of the observed jet in a single-jet inclusive calculation. Variations in these quantities can lead to significant changes in the normalization and to a lesser extent shapes of the resulting predictions. Thus, predictions of absolute normalizations are subject to large theoretical uncertainties

 ©1989 The American Physical Society

when the leading-logarithm approximation is used. Relative normalizations, however, are less subject to these uncertainties. Representative examples of such calculations are reviewed in Ref. 8.

In order to achieve a higher level of theoretical precision, it is necessary to go beyond the leading-logarithm approximation; at least one must include the next-to-leading logarithms. In many instances such calculations show a less dramatic dependence on the renormalization and factorization scale choices than is the case when the leading logarithms alone are used. However, retaining subleading logarithms leads, in general, to more complex calculations. Furthermore, it is often difficult to calculate the quantities which are observable in a given experiment, taking into account the acceptances of the detector, different jet definitions, etc. In addition, each new observable requires a new calculation. For this reason, we have utilized a different technique for performing next-to-leading-logarithm calculations which is based on a Monte Carlo approach.[9,10] This technique is straightforward to implement and does not require an inordinate amount of computer time. Furthermore, new observables can be calculated by simply modifying the quantities to be histogrammed. The additional theoretical expressions are neither long nor complicated.

Utilizing such a scheme has allowed us to study the modifications of a variety of observables in jet photoproduction. Interestingly enough, different types of cross sections have significantly different corrections when going from the leading-logarithm to the next-to-leading-logarithm approximation. There is not, for example, a simple multiplicative "K factor" which corrects a single subprocess—there is a dependence on the type of observable being calculated. Several examples of this phenomenon are discussed. In particular, it is possible to find cross sections, e.g., a semi-inclusive two-jet cross section, which shows very little variation as the renormalization and factorization scales are changed. This is the first time that such a detailed comparison of different observables has been possible in the framework of a next-to-leading-logarithm calculation.

The remainder of the paper is as follows. In Sec. II we review the leading-logarithm calculations and establish some basic notation. Section III contains a review of the basic techniques used in the Monte Carlo next-to-leading-logarithm calculation and a thorough discussion of the results obtained using the techniques presented. Section IV is reserved for a summary of our conclusions. An appendix is provided which contains expressions used in the construction of the Monte Carlo program.

II. LEADING-LOGARITHM FORMALISM

One of the advantages of jet photoproduction is that the pointlike component involves only one hadronic distribution function: namely, that of the target. The remaining four-vectors of the beam and the two final-state jets are, in principle, subject to direct experimental determination. Of course, this ignores subtleties associated with the identification algorithm used for the jets and problems of subtracting the photon structure-function contribution. However, these problems diminish in magnitude as the hard-scattering transverse momentum is increased.

Another interesting feature of jet photoproduction is the possibility of observing the interplay between the pointlike and structure-function components.[1] They are each characterized by distinctly different angular distributions, a feature which can aid in their separation.[7] For the purpose of this analysis we shall use a set of simple parametrizations of the parton distributions in a photon which were obtained by solving the relevant inhomogeneous Altarelli-Parisi equations using moments and then fitting simple parametrizations to the results. The parametrizations are

$$xG_{q_i/\gamma}(x,Q^2)=F\left\{e_i^2(1.81-1.67x+2.16x^2)\times\frac{x^{0.70}}{1-0.4\ln(1-x)}+0.0038(1-x)^{1.82}x^{-1.18}\right\} \tag{1a}$$

and

$$xG_{g/\gamma}(x,Q^2)=0.194F(1-x)^{1.03}x^{-0.97}\,, \tag{1b}$$

where $F=(\alpha/2\pi)\ln(Q^2/\Lambda^2)$ and e_i is the fractional charge on the quark q_i. Throughout this paper we shall use $\Lambda=200$ MeV.

An alternative set of parametrizations is contained in Ref. 11. In this reference, in addition to the leading QCD piece, the authors have included a vector-dominance-motivated component which is required in order to describe the photon structure function for Q^2 values in the few GeV^2 range. Such a component does not play a significant role in the kinematic region which we shall be considering since it gives rise to parton x distributions which are peaked at smaller values of x than are the leading QCD contributions. Thus, the vector-dominance contribution gives rise to a steeper jet p_T spectrum than the other sources we are considering.[1] Indeed, a direct comparison of the results from Eq. (1) and the distributions of Ref. 11 shows that they are very similar in the Q^2 region we shall be investigating.

For the target nucleon, the parton distributions of Ref. 12 will be utilized. All of the predictions shown here correspond to the set 1 distributions with $\Lambda=200$ MeV. In addition, the leading-logarithm predictions have been obtained using the one-loop expression for α_s with four flavors.

For the convenience of the reader, the expressions for selected observables are given below. A more detailed review of the relevant kinematics and formalism can be found in the Appendix of Ref. 8. An additional discussion of the theoretical formalism specific to leading-logarithm calculations for jet photoproduction can be found in Sec. II of Ref. 1. In the following, collinear kinematics for the incoming partons is assumed. It is possible to include effects of nonzero transverse moments for the colliding partons in a model-dependent way, as reviewed in Ref. 8. However, in this case we are dealing

with only one incoming hadron so such effects are reduced as compared to the hadron-hadron case. Furthermore, the next-to-leading-logarithm calculations to be discussed in the next section contain a portion of such effects due to initial-state bremsstrahlung.

The single-jet invariant cross section can be written as

$$E\frac{d^3\sigma}{dp^3}(\gamma B \to \text{jet}+X) = \sum_{abcd}\int dx_a dx_b G_{a/\gamma}(x_a)G_{b/B}(x_b) \times \frac{\hat{s}}{\pi}\frac{d\sigma}{d\hat{t}}(ab\to cd)\delta(\hat{s}+\hat{t}+\hat{u}) . \quad (2)$$

Here, and in the following, the expression has been written for the case of the photon-structure-function component. For the pointlike component the sum over $G_{a/\gamma}(x_a)$ should be replaced by $\delta(x_a-1)$. The caret symbol has been used to designate the Mandelstam variables which pertain to the parton-parton system. They may be written in terms of x_a, x_b, and the observed jet transverse momentum and rapidity p_T and y as

$$\hat{s}=x_a x_b s, \quad \hat{t}=-x_a p_T\sqrt{s}\,e^{-y}, \quad \hat{u}=-x_b p_T\sqrt{s}\,e^{y} .$$

The x_b integration may be performed using the delta function, with the result that

$$E\frac{d^3\sigma}{dp^3}(\gamma B\to\text{jet}+X)=\sum_{abcd}\int_{x_a^{\min}}^{1} dx_a G_{a/\gamma}(x_a)G_{b/B}(x_b) \times\frac{2}{\pi}\frac{x_a x_b}{2x_a-x_T e^{y}} \times\frac{d\sigma}{d\hat{t}}(ab\to cd) , \quad (3)$$

where $x_b=x_a x_T e^{-y}/(2x_a-x_T e^{y})$, $x_a^{\min}=x_T e^{y}/(2-x_T e^{-y})$, and $x_T=2p_T/\sqrt{s}$.

At this level of approximation, all of the events considered will have two wide-angle jets. Let M be the dijet invariant mass and $\cos(\theta^*)$ be the cosine of the angle of the dijet axis with respect to the beam direction in the dijet rest frame. Then, one can write

$$\frac{d^2\sigma}{dM^2 d\cos(\theta^*)}(\gamma B\to j_1+j_2+X) = \sum_{abcd}\int_{M^2/s}^{1} dx_a G_{a/\gamma}(x_a)G_{b/B}(x_b)\frac{x_b}{2}\frac{d\sigma}{d\hat{t}}(ab\to cd) . \quad (4)$$

In this case, $M^2=x_a x_b s$ and $\hat{t}=-(M^2/2)[1-\cos(\theta^*)]$.

The preceding expressions can be used to obtain an estimate of the behavior of the various components of the leading-logarithm calculation. For example, in Fig. 1 the single-jet invariant cross section is shown versus p_T. Unless otherwise stated, $Q^2=p_T^2$ has been used. Both the pointlike and structure-function components are shown, together with the sum. The structure-function component has a steeper falloff, due to the additional convolution associated with the parton distributions in the photon. The flatter pointlike component dominates for $p_T>6$ GeV, illustrating the effect of depositing all of the photon's energy into the subprocess. This latter point can be seen again in Fig. 2 where the single-jet invariant cross section is shown versus the γ-proton center-of-mass rapidity at $p_T=6$ GeV. The pointlike contribution is more sharply peaked in the forward direction (positive y) than is the structure-function contribution. This suggests that if one wants to suppress the structure-function component in order to better study the pointlike part, then the detector should be optimized for forward values of y.

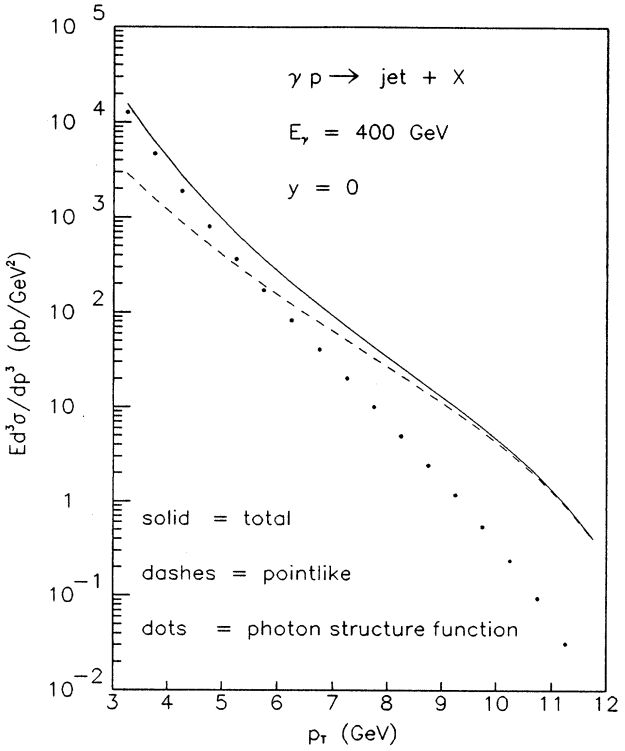

FIG. 1. The inclusive single-jet invariant cross section in the leading-logarithm approximation vs p_T at $y=0$ with a photon beam energy of 400 GeV. The total, pointlike, and structure-function components are shown by the solid, dashed, and dotted lines, respectively.

It is of interest to also examine the dijet angular distribution as a function of mass. The structure-function component consists of the usual QCD qq, qg, and gg two-body subprocesses which contribute to hadron-hadron jet production. The resulting angular distribution will thus be sharply peaked in the forward direction, reflecting the dominance of the t-channel-exchange processes. However, for the pointlike component the t-channel component plays a lesser role, due to the presence of a significant s-channel term in the Compton subprocess. Thus, the pointlike term is expected to be less steep. As the mass of the dijet system is increased, the relative amount of the pointlike contribution will increase. Therefore, there should be a flattening of the angular distribution. This effect should be very pronounced

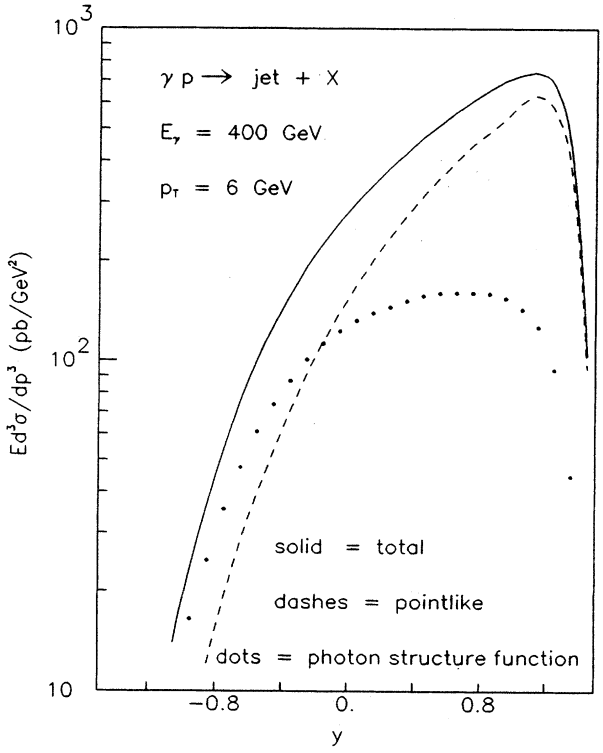

FIG. 2. The inclusive single-jet invariant cross section in the leading-logarithm approximation vs y at $p_T=6$ GeV with a photon beam energy of 400 GeV. The total, pointlike, and structure-function components are shown by the solid, dashed, and dotted lines, respectively.

in the kinematic range available at HERA (Ref. 7). The effect should also be present for fixed-target photoproduction, as can be seen in Fig. 3 where the results are shown for two values of the dijet mass. The distributions are shown for pointlike and structure-function contributions separately, as well as for their sum. In each instance the angular distributions have been normalized to unity at $\cos(\theta^*)=0$. The different shapes of the two contributions are readily apparent. Neither distribution by itself shows a significant variation with increasing dijet mass. However, the varying admixture of the two components yields a change in shape for the sum as the dijet mass is increased. It may be possible to separate the two components by vetoing events with a clear beam jet. In this instance a sample dominated by the pointlike component should be obtained with a characteristically flatter angular distribution.

As discussed in the Introduction, the predictions shown thus far depend on the choices made for the renormalization and factorization scales, thus far taken to both be p_T^2. In order to reduce this sensitivity, we need to go beyond the leading-logarithm approximation. This is the topic of the next section.

III. NEXT-TO-LEADING-LOGARITHM FORMALISM

In the previous section we have discussed a typical leading-logarithm calculation for jet photoproduction. In that case, the hard-scattering subprocesses for the pointlike part were calculated to $O(\alpha\alpha_s)$ and higher-order contributions were included via the scaling violations in the target hadron's parton distribution functions. For the structure-function component the hard-scattering subprocesses are $O(\alpha_s^2)$ while the photon structure function is $O(\alpha/\alpha_s)$ so that the results are of the same order as for the pointlike case. Both of these constitute all-orders calculations, but only the leading logarithm from each of the terms beyond $O(\alpha\alpha_s)$ is retained. Such a treatment has been shown to successfully describe a wide variety of high-p_T data once the renormalization and factorization scales have been chosen appropriately. The purpose of this section is to describe a calculation in which the hard-scattering contributions to the pointlike component are calculated to $O(\alpha\alpha_s^2)$; this process will also pick up some subleading contributions to the

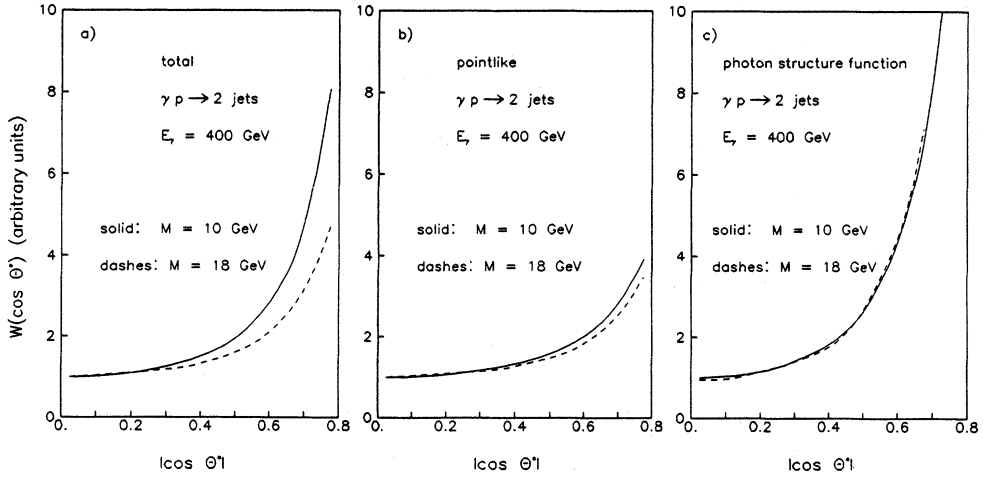

FIG. 3. The normalized two-jet angular distribution in the leading-logarithm approximation for dijet masses of 10 and 18 GeV vs $|\cos(\theta^*)|$ for $E_\gamma=400$ GeV. The total, pointlike, and structure-function contributions are shown separately.

structure-function component, as well.

As an introduction to the technique, it will be useful to first review the problems associated with using Monte Carlo techniques for a next-to-leading-logarithm calculation and our particular methods for solving them.[9,10] After that, the details of the calculation will be presented. Some of the longer expressions have been collected in an appendix. By including terms up to $O(\alpha\alpha_s^2)$ in the hard-scattering cross section, a number of new contributions arise. These are the one-loop contributions to $\gamma q \to gq$ and $\gamma g \to q\bar{q}$ and the three-body subprocesses $\gamma q \to gqg$, $\gamma q \to qq\bar{q}$, $\gamma q \to qq'\bar{q}'$, and $\gamma g \to q\bar{q}g$. As is usual with calculations of this type, there will be a number of singularities associated with the new contributions. The ultraviolet singularities associated with the one-loop contributions have been regulated using the method of dimensional regularization[13] and subtracted using the modified minimal-subtraction ($\overline{\text{MS}}$) scheme.[14] Similarly, dimensional regularization has been used in treating the infrared, soft, and collinear divergences.

The basic idea rests upon the fact that for a suitably defined inclusive observable, the infrared singularities associated with the one-loop contributions will cancel against the soft singularities associated with the three-body tree graphs. Furthermore, the collinear singularities from initial-state radiation and pair creation can be factorized and included in the parton distribution functions. The hard collinear singularities from final-state radiation and pair creation will cancel against corresponding singularities from the one-loop graphs. The basic challenge, then, is to find a way of ensuring that all of the required cancellations can take place within the context of a Monte Carlo calculation.

For the purpose of this section, the four-vectors of the two-body and three-body subprocesses will be labeled by $p_1+p_2 \to p_3+p_4$ and $p_1+p_2 \to p_3+p_4+p_5$, respectively. Lorentz scalars $s_{ij}=(p_i+p_j)^2$ and $t_{ij}=(p_i-p_j)^2$ will be used.

The method chosen for this calculation is to introduce two cutoff parameters, δ_s and δ_c, whose purpose is to allow the separation of the regions of phase space which contain the singularities. For the three-body subprocesses, the soft singularities are associated with the phase-space region where one final-state gluon becomes soft. We define the soft region to be that where the relevant parton energy in the subprocess rest frame becomes less than $\delta_s\sqrt{s_{12}}/2$. If δ_s is chosen to be sufficiently small, then the relevant three-body subprocesses can be evaluated using the soft-gluon approximation wherein the gluon energy is set to zero in the numerator of the expression. The resulting expression is then easily integrated over the soft region of phase space. At this stage, this integrated soft piece contributes to the two-body part which contains the one-loop terms. The soft and infrared singularities can then be canceled explicitly. Next, the collinear regions of phase space are defined to be those where any invariant (s_{ij} or t_{ij}) becomes smaller in magnitude than $\delta_c s_{12}$. If δ_c is chosen sufficiently small, then in each collinear region the relevant subprocess can be evaluated using the leading-pole approximation. The result is easily integrated in n dimensions, thereby explicitly displaying the collinear singularities. These are then factorized and included in the relevant structure functions or canceled with corresponding singularities in the two-body expressions. At this point, the remainder of the three-body phase space contains no singularities and the subprocesses can be evaluated in four dimensions.

The calculation now consists of two pieces—a set of two-body contributions and a set of three-body contributions. Each set consist of finite parts, all singularities having been canceled, subtracted, or factorized. However, each part depends separately on the two theoretical cutoffs δ_s and δ_c. Each by itself has no intrinsic meaning. In fact, for very small values of δ_s we shall see that logarithms of the cutoff will force the two-body contribution to become negative. However, when the two- and three-body contributions are combined to form a suitably inclusive observable, e.g., an inclusive single-jet invariant cross section, all dependence on the cutoffs will cancel. It will turn out that the answers are stable against variations of these cutoffs over quite a wide range. Physically, this is as it should be. The cutoffs merely serve to distinguish the regions where the phase-space integrations are done by hand from those where they are done by Monte Carlo simulations. When the results are added together, the precise location of the boundary between the two regions is not relevant. Thus, the answer becomes independent of the cutoffs. Of course, this is valid only over a certain range of cutoff values. The cutoffs must be sufficiently small that the soft-gluon and leading-pole approximations are valid in the regions near the edge of phase space where they are used. Furthermore, when these regions are integrated over, terms which vanish in the limit of zero cutoff are discarded. This provides an additional reason for requiring small cutoffs. Finally, the cutoffs must be chosen so that the experimental cuts placed on an observable do not interfere with the cancellation referred to above. In general, this also requires small values of the cutoffs. The results reported below are stable to variations in the cutoffs, thus providing a check on the calculation. Calculating a different observable simply requires forming the appropriate histogram. This flexibility is the major advantage of the technique. The price paid for this ease of use is that two sets of Monte Carlo "events" must be generated and added together. In practice, this is not a major imposition.

At this point, a survey of some typical results will serve to outline the versatility and convenience of this approach. The detailed expressions utilized in the calculational scheme outlined above are given in the Appendix. For the first example, consider the single-jet invariant cross section with a cut requiring that there be no jet with rapidity greater than 2. This cut eliminates the beam jet from the photon-structure-function contribution so that the result is just the pointlike part, calculated to $O(\alpha\alpha_s^2)$. In addition, a jet definition must be chosen which will coalesce two partons which are nearly parallel, since one cannot resolve such collinear jets. We have chosen to combine the four-vectors of any pair of partons for which $\Delta R=\sqrt{(\Delta y)^2+(\Delta\phi^2)}<1$ where Δy and $\Delta\phi$ are the differences in rapidity and azimuthal angle of the jets.

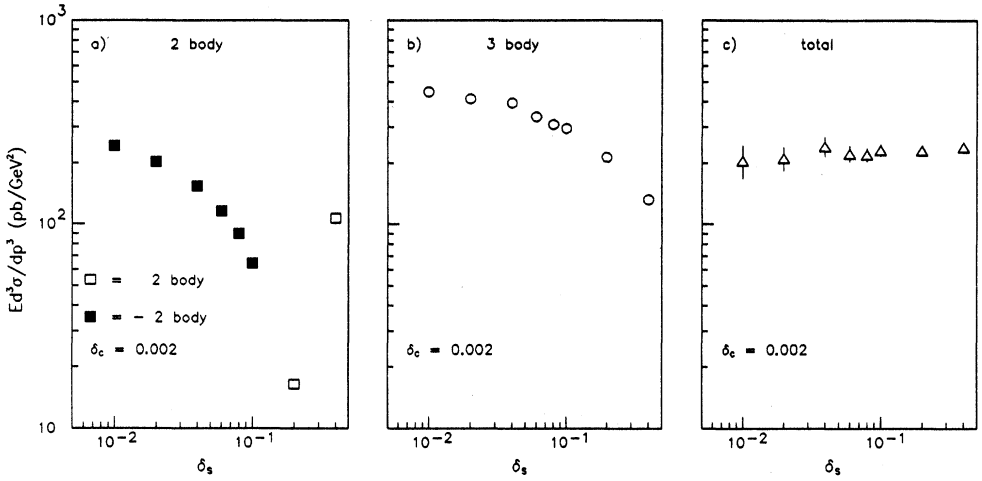

FIG. 4. The inclusive single-jet invariant cross section calculated with a forward rapidity cut so as to eliminate the structure-function contribution. The cross section is shown for the point $y=0$, $p_T=6$ GeV, and $E_\gamma=400$ GeV. The two-body and three-body contributions together with their sum are shown vs the soft cutoff δ_s at $\delta_c=0.002$.

In Fig. 4 the results at $y=0$, $p_T=6$ GeV, and $E_\gamma=400$ GeV are shown versus the soft cutoff δ_s for a fixed value of the collinear cutoff δ_c. The two-body and three-body contributions are shown separately, together with the sum. Note that as δ_s is decreased the two-body contribution becomes negative. This is a result of the explicit logarithmic dependence of the two-body part on δ_s and does not correspond to the behavior of a physical cross section. On the other hand, the three-body part shows an increase as δ_s decreases. The net result for the sum of the two terms is constant, within the Monte Carlo statistics, over the range of δ_s shown. Figure 5 is a similar set of plots, this time as a function of δ_c with $\delta_s=0.05$. Again, the cancellation takes place, leaving a result independent of the cutoffs. This cutoff independence is a necessary, though not sufficient, check on the calculation.

Next, in Fig. 6 results are shown for the inclusive single-jet invariant cross section at $y=0$ for two values of p_T. The forward rapidity cut has again been used to remove the structure-function contribution. The results are shown versus the parameter n where both the renormalization and factorization scales have been parametrized as $Q^2=np_T^2$. For three-body final states, the largest p_T in the event has been used. Both the leading-logarithm and next-to-leading-logarithm results are shown. Note that the two-loop running coupling has been used for both the leading- and next-to-leading-logarithm results, thereby providing a consistent expansion parameter so that one can judge the degree of convergence represented by the results. Over the range of scales shown, the results at $p_T=6$ GeV show an increase of between a factor of 1.5 and 2 when the next-to-leading contributions are retained. For this p_T value the dependence on n is approximately the same for the leading- and

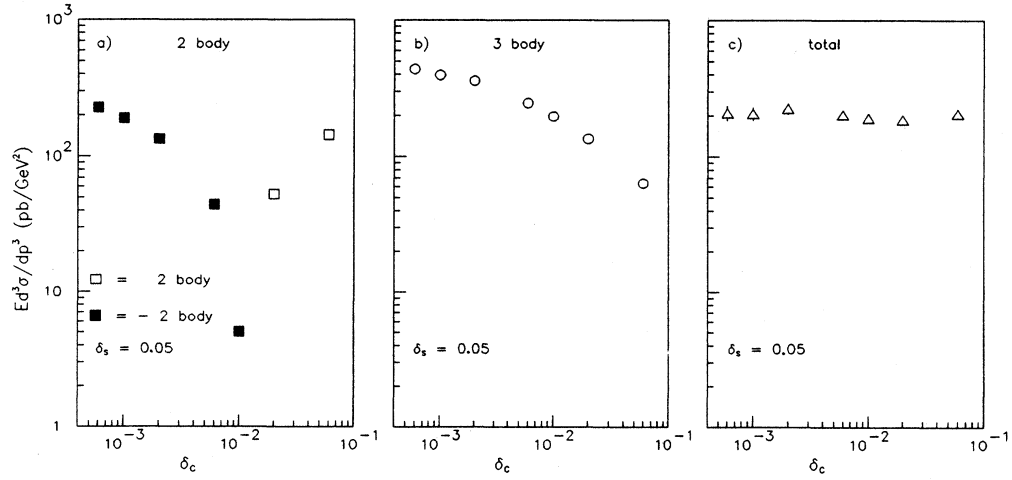

FIG. 5. The same as Fig. 4 except the results are shown vs δ_c for $\delta_s=0.05$.

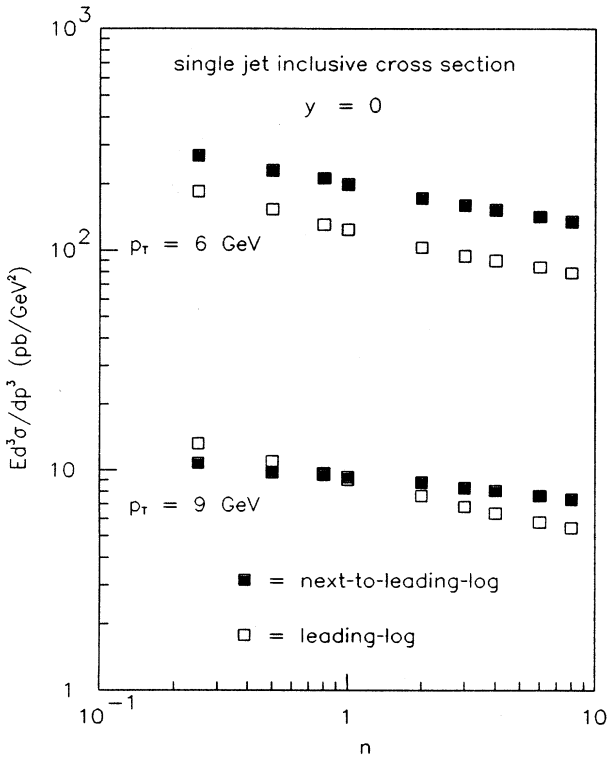

FIG. 6. The inclusive single-jet invariant cross section is shown at $y=0$ and $E_\gamma=400$ GeV for $p_T=6$ and 9 GeV vs n where $Q^2=np_T^2$ has been used for both the factorization and renormalization scales. Both the leading-logarithm and next-to-leading-logarithm results are shown.

next-to-leading results. On the contrary, at $p_T=9$ GeV the next-to-leading result is much flatter than the leading-logarithm result. This decreased sensitivity to variations of the scales is one of the hoped for features of the next-to-leading-logarithm calculation. However, one may well ask why the corrections become large at low values of p_T and why the sensitivity to the change of scales is larger. To investigate this point we have decomposed the answer into its component parts—the leading-logarithm, soft, and collinear parts of the two-body contribution and the positive-definite three-body part. Recall that these separations depend on the cutoffs δ_s and δ_c. Therefore, the relative size of the contributions is not what is important, but rather one must look at the systematic behavior versus p_T of the various components. It was observed that as the p_T is increased, the three-body part falls off more rapidly than the net two-body contribution. This can be understood by realizing that the typical configuration for generating at least one high-p_T parton is to have one parton balanced by two in the opposite hemisphere sharing the recoil and, therefore, having smaller p_T values. It is relatively rare to have roughly equal values for all three transverse momenta, as opposed to the two-body events where the transverse momenta are equal. This means that the ratio of high-p_T to low-p_T jets is smaller for three-body events than for two-body events. Next, notice that the dependences on Q^2 of the leading-logarithm and three-body parts are similar, with both having a monotonic decrease with increasing Q^2. At the lower values of p_T the enhanced importance of the three-body contribution leads to a large positive-definite addition to the leading-logarithm result which has the same type of Q^2 dependence. At the higher values of p_T the three-body contribution decreases in importance and the

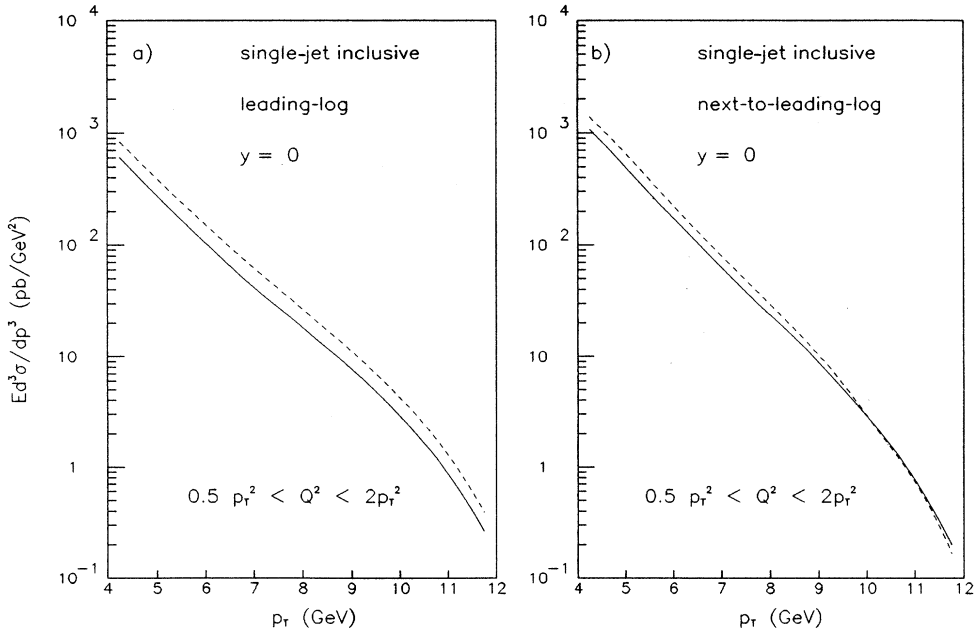

FIG. 7. The leading-logarithm and next-to-leading-logarithm results for the inclusive single-jet invariant cross section shown for $Q^2=0.5p_T^2$ (dashed curves) and $Q^2=2p_T^2$ (solid curves) at $y=0$ and $E_\gamma=400$ GeV.

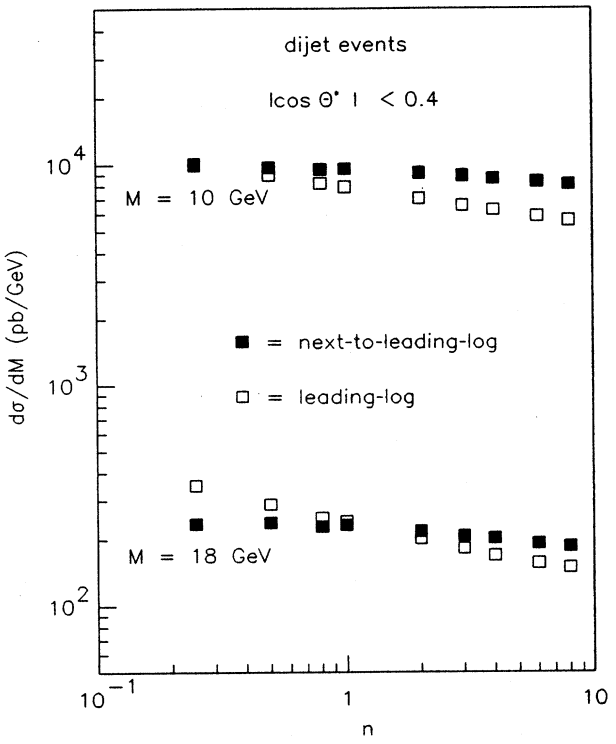

FIG. 8. Same as Fig. 6 except for the dijet mass distribution at $M = 10$ and 18 GeV.

compensating logarithms in the $O(\alpha\alpha_s^2)$ part become relatively more important, yielding the flatter dependence shown in Fig. 6.

Figure 7 contains predictions for the inclusive single-jet invariant cross section at $y = 0$ vs p_T in both the leading- and next-to-leading-logarithm approximations. The results are given for both $Q^2 = 2p_T^2$ (solid curves) and $0.5p_T^2$ (dashed curves). In the leading-logarithm case, the dashed curve lies approximately 50% above the solid curve over the entire p_T range shown. In the next-to-leading-logarithm case the two curves actually cross near $p_T = 10$ GeV resulting in a much smaller variation with Q^2 than in the leading-logarithm case over a substantial portion of the p_T range shown.

The preceding discussion indicates that the sensitivity of the next-to-leading-logarithm predictions to variations in Q^2 depends on the value of p_T and that this p_T dependence can be traced, in part, to the fact that for the three-body part there are three entries per event in the inclusive cross section. This suggests that the situation might be different for an observable involving two, and only two, jets. As an example, consider the dijet mass distribution $d\sigma/dM$ where M is the invariant mass of the dijet system. Again, a forward rapidity cut requiring that each jet have $y < 2$ has been used to remove the structure-function contribution. In addition, we must examine how the three-body part will contribute to a dijet cross section. As for the single-jet calculation, any pair of partons with $\Delta R < 1$ is combined to form a single jet. Next, if the three jets were sufficiently isolated so that there was no coalescence, they are ordered in terms of decreasing p_T with $p_{T_1} > p_{T_2} > p_{T_3}$. If $p_{T_3} < 2$ GeV, then the three-body event is included in the dijet cross section. The idea is that with this small value of p_T, the jet would escape detection and the event would appear as a dijet event. This definition is certainly not unique, and other definitions are equally suitable. All that is required is that the definitions be constructed in such a way that one avoids resolving nearly collinear jets and that sufficiently soft jets are not counted. This is similar in spirit to the

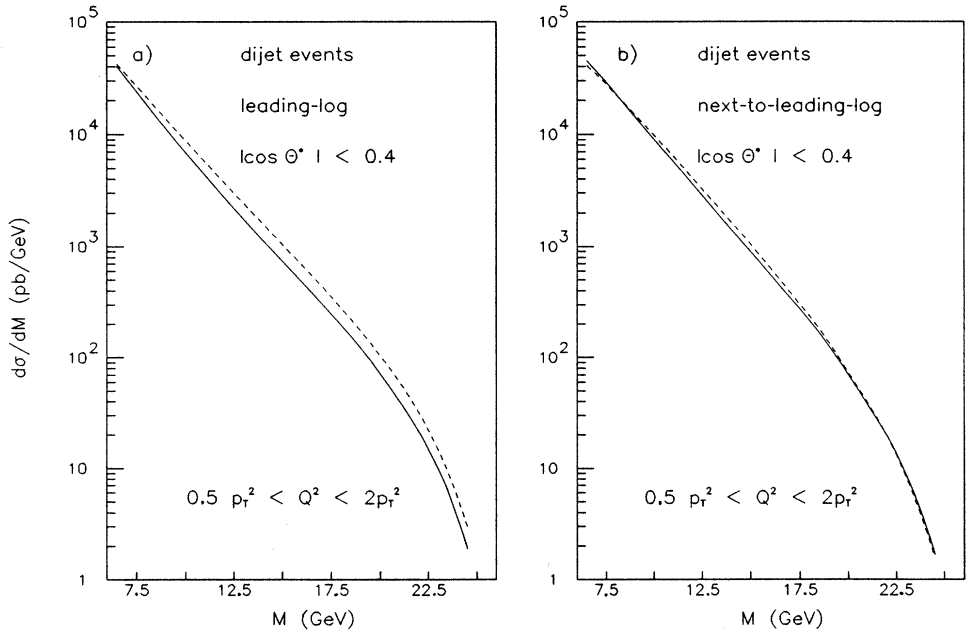

FIG. 9. Same as Fig. 7 except for the dijet mass distribution.

usual Sterman-Weinberg jet definition familiar from e^+e^- studies.[15]

In addition to the cuts mentioned above, we have also required that $|\cos(\theta)^*| < 0.4$ where, for two-body events, θ^* is the scattering angle in the dijet rest frame. For three-body events, $\cos(\theta)^*$ is determined by first boosting to the frame in which the dijet system has no net momentum along the beam direction. The value of $|\cos(\theta^*)|$ is determined for each of the two jets in this frame and the average of the two values is used.

In Fig. 8 the results for $d\sigma/dM$ are shown for two values of the dijet mass versus n, as was shown for the single-jet case in Fig. 6. In this instance we see that the next-to-leading-logarithm results are significantly less sensitive than the leading-logarithm results to variations of the Q^2 definition. This is shown again in Fig. 9 where the dijet mass distributions are displayed for two values of Q^2. The lack of dependence on the Q^2 definition for the next-to-leading-logarithm calculation is striking. The reduction in sensitivity is due largely to the reduced role played by the three-body contribution. Those events passing all the cuts make only one entry in the histogram rather than two or three as was the case in the inclusive single-jet calculation.

The contrasting degree of sensitivity to Q^2 definitions shown by the single and dijet calculations is an important result. If the dominant effect of the next-to-leading-logarithm terms was to enhance the two-body contribution via the so-called π^2 terms, then the ratio of the leading- and next-to-leading-logarithm results would be similar in the two calculations, as would the sensitivity to the Q^2 choice. That this is not the case clearly underscores the importance of performing complete calculations which can be precisely tailored to the appropriate definition of the experimental observable in question.

IV. SUMMARY AND CONCLUSIONS

The example of jet photoproduction presented here has many interesting features which soon will be studied in at least one experiment. The interplay between the pointlike and structure-function contributions should show up to some extent in the rapidity and transverse-momentum dependence of the single-jet yield. A more sensitive effect may be observed in the dijet angular distribution which is significantly flatter for the pointlike part than for the structure-function contribution.

As experiments continue to collect high-statistics samples of hard-scattering events for processes in new energy regions and for new types of observables, the focus of these studies will shift from testing QCD to new areas where the hard scattering can be used to learn new physics. Examples include improved determinations of parton distributions, limits on quark substructure, and new particle searches. These topics will require improved levels of precision for the theoretical calculations which, in turn, means performing next-to-leading-logarithm calculations for a wide variety of observables. With conventional analytic techniques each observable requires a new calculation and it becomes difficult to match different jet definitions, experimental cuts, etc. In this paper we have shown how a Monte Carlo–based technique can be used to develop a flexible and easy-to-use program for calculating observables with next-to-leading-logarithm accuracy in jet photoproduction. The methods can easily be extended to other reactions, as well.

In order to demonstrate the flexibility of this technique, results for various one- and two-jet observables were presented, some of which included cuts to eliminate the photon-structure-function contribution in favor of the pointlike term. The observables are insensitive to the values chosen for the theoretical soft and collinear cutoffs used in intermediate stages of the calculation, a necessary though not sufficient constraint on the validity of the results. It was demonstrated that the nature of the corrections to the leading-logarithm results depends very much on the observable in question. Furthermore, the sensitivity to the factorization and renormalization scales depends on the observable and on the kinematic region in question. The net $O(\alpha\alpha_s^2)$ corrections to the single-jet inclusive cross section were positive definite and of the same order as the leading-logarithm results for a wide range of scale choices, when the renormalization and factorization scales were chosen to be equal. On the other hand, the corresponding corrections to a particular two-jet cross section were much smaller and the resulting predictions were very stable with respect to choices of the scales. This result was easily explained after examining the various contributions to each cross section. The lesson appears to be that some observables can be calculated with a higher degree of precision than others. This is an interesting result which should be borne in mind when analyzing data and comparing to theoretical predictions.

ACKNOWLEDGMENTS

This work was supported in part by the U.S. Department of Energy.

APPENDIX

In this appendix the input expressions used in the next-to-leading-logarithm Monte Carlo calculation are summarized. The techniques used here are discussed in more detail in Refs. 9 and 10.

The basic structure of the calculation depends on whether or not events with beam jets are included. If beam-jet events are vetoed, for example by rejecting events with a jet near the beam direction (as was done for some of the calculations presented in this paper), then the calculation involves two-body and three-body contributions, but no photon-structure-function contribution. On the other hand, if beam jet events are included, then the contribution from the photon structure function must also be included. The expressions for these three types of contributions are summarized in the following sections.

1. Two-body contributions

In this section the Mandelstam variables s, t, and u are the same as s_{12}, t_{13}, and t_{23}. In addition, it is convenient to scale t in order to obtain a variable $v = 1 + t/s$ which ranges from 0 to 1. In terms of these variables the full contribution has the form

$$\sigma_{2\text{ body}}^{\text{NLL}}(\gamma N\to\text{jets}+X)=\sum_q\int\left[G_{q/N}(x_b,M^2)\frac{d\sigma^{\text{NLL}}}{dv}(\gamma q\to gq)+\frac{d\tilde{\sigma}}{dv}(\gamma q\to gq)\right.$$
$$\left.+G_{g/N}(x_b,M^2)\frac{d\sigma^{\text{NLL}}}{dv}(\gamma g\to q\bar{q})+\frac{d\tilde{\sigma}}{dv}(\gamma g\to q\bar{q})\right]dv\,dx_b\ . \tag{A1}$$

The two contributions labeled $d\sigma^{\text{NLL}}/dv$ include both the two-body subprocesses calculated to $O(\alpha\alpha_s^2)$ (Ref. 16), the soft contributions from the $O(\alpha\alpha_s^2)$ three-body processes, and the contributions from the hard collinear singularities in the final state. The singularities associated with the initial-state parton distributions have been factorized and absorbed into the initial parton distributions. The terms denoted by $d\tilde{\sigma}/dv$ are the remnants of the hard collinear singularities after the factorization process has been performed.

The individual terms in Eq. (A1) are displayed below:

$$\frac{d\sigma^{\text{NLL}}}{dv}(\gamma q\to gq)=\alpha_s(\mu^2)CT_0^{\gamma q}+\frac{\alpha_s^2(\mu^2)}{2\pi}C(T_0^{\gamma q}A_0+B_0)\ , \tag{A2}$$

with

$$A_0=-\tfrac{1}{6}(11N_C-2N_F)\ln\frac{s}{\mu^2}+\frac{N_F}{3}(\ln\delta_c-\tfrac{5}{3})-N_C(2\ln\delta_s+\tfrac{11}{6})\ln\delta_c$$
$$+(2C_F-N_C)\left[\tfrac{1}{2}\ln^2\frac{t}{u}+\tfrac{1}{2}\ln^2\frac{-t}{s}+2\ln\delta_s\ln\frac{-t}{s}+\text{Li}_2\frac{-u}{s}\right]$$
$$+N_C\left[\tfrac{1}{2}\ln^2\frac{-u}{s}+2\ln\delta_s\ln\frac{-u}{s}+\text{Li}_2\frac{-t}{s}+\ln^2\delta_s+\frac{67}{18}-\frac{\pi^2}{2}\right]$$
$$+C_F\left[\frac{\pi^2}{3}-\frac{7}{2}+3\ln^2\delta_s-\ln\delta_c(2\ln\delta_s+\tfrac{3}{2})+(\tfrac{3}{2}+2\ln\delta_s)\ln\frac{s}{M^2}+\lambda\left[\frac{\pi^2}{2}+\frac{9}{2}-\ln^2\delta_s+\tfrac{3}{2}\ln\delta_s\right]\right]\ ,$$

$$B_0=-3C_F\frac{s}{u}\ln\frac{-u}{s}-\tfrac{1}{2}(2C_F-N_C)\left[\left[2+\frac{u}{s}\right]\left[\pi^2+\ln^2\frac{t}{u}\right]+\left[2+\frac{s}{u}\right]\ln^2\frac{-t}{s}\right]\ ,$$

$$T_0^{\gamma q}=-\left[\frac{s}{u}+\frac{u}{s}\right],\ \text{and}\ C=\frac{2\pi\alpha}{s}e_q^2C_F\ .$$

Here δ_s and δ_c are the soft and collinear cutoff parameters introduced in Sec. III, $\text{Li}_2(x)$ is the dilogarithm function, M^2 is the factorization scale, and μ^2 is the renormalization point. In addition, e_q is the quark fractional charge, $C_F=\frac{4}{3}$ is the quark-gluon vertex color factor, N_C is the number of colors, and N_F is the number of active quark flavors. The parameter λ depends on the factorization convention chosen. For this calculation, $\lambda=1$ has been used, as is discussed below. The terms for $\gamma g\to q\bar{q}$ are similar:

$$\frac{d\sigma^{\text{NLL}}}{dv}(\gamma g\to q\bar{q})=\tfrac{3}{8}\alpha_s(\mu^2)CT_0^{\gamma g}+\frac{3}{8}\frac{\alpha_s^2(\mu^2)}{2\pi}C(T_0^{\gamma g}A_0+B_0)\ , \tag{A3}$$

where

$$A_0=\tfrac{1}{6}(11N_C-2N_F)\ln\frac{\mu^2}{M^2}+C_F\left[\ln^2\frac{-t}{s}+\ln^2\frac{-u}{s}+2\ln^2\delta_s-4\ln\delta_c\ln\delta_s-3\ln\delta_c\right]$$
$$+N_C\left[-\tfrac{1}{2}\ln^2\frac{tu}{s^2}+2\ln^2\delta_s+2\ln\delta_s\ln\frac{s}{M^2}+2\ln\delta_s\ln\frac{tu}{s^2}+\tfrac{1}{2}\ln^2\frac{t}{u}\right]\ ,$$

$$B_0=3C_F\left[\frac{t}{u}\ln\frac{-u}{s}+\frac{u}{t}\ln\frac{-t}{s}\right]+\tfrac{1}{2}(2C_F-N_C)\left[2\ln\frac{tu}{s^2}+\left[2+\frac{u}{t}\right]\ln^2\frac{-u}{s}+\left[2+\frac{t}{u}\right]\ln^2\frac{-t}{s}\right]\ ,$$

and

$$T_0^{\gamma g}=\left[\frac{t}{u}+\frac{u}{t}\right]\ .$$

The remnants of the factorization of the hard collinear singularities are given by

$$\frac{d\tilde{\sigma}}{dv}(\gamma q\to gq)=\frac{\alpha_s^2(\mu^2)}{2\pi}CT_0^{\gamma q}\left\{\int_{x_b}^{1-\delta_s}\frac{dz}{z}G_q(x_b/z,M^2)\left[P_{qq}(z)\ln\left[\frac{1-z}{z}\delta_c\frac{s}{M^2}\right]-P'_{qq}(z)-\lambda F_{qq}(z)\right]\right.$$
$$\left.+\int_{x_b}^{1-\delta_s}\frac{dz}{z}G_g(x_b/z,M^2)\left[P_{qg}(z)\ln\left[\frac{1-z}{z}\delta_c\frac{s}{M^2}\right]-P'_{qg}(z)-\lambda F_{qg}(z)\right]\right\} \quad \text{(A4)}$$

and

$$\frac{d\tilde{\sigma}}{dv}(\gamma g\to q\bar{q})=\frac{3}{8}\frac{\alpha_s^2(\mu^2)}{2\pi}CT_0^{\gamma g}\left\{\int_{x_b}^{1-\delta_s}\frac{dz}{z}G_g(x_b/z,M^2)\left[P_{gg}(z)\ln\left[\frac{1-z}{z}\delta_c\frac{s}{M^2}\right]-P'_{gg}(z)-\lambda F_{gg}(z)\right]\right.$$
$$\left.+\int_{x_b}^{1-\delta_s}\frac{dz}{z}G_q(x_b/z,M^2)\left[P_{gq}(z)\ln\left[\frac{1-z}{z}\delta_c\frac{s}{M^2}\right]-P'_{gq}(z)-\lambda F_{gq}(z)\right]\right\}. \quad \text{(A5)}$$

The Altarelli-Parisi splitting functions in $4-2\epsilon$ dimensions are, for $z<1$,

$$P_{qq}(z,\epsilon)=C_F\left[\frac{1+z^2}{1-z}-\epsilon(1-z)\right],$$
$$P_{qg}(z,\epsilon)=\frac{1}{2(1-\epsilon)}[z^2+(1-z)^2-\epsilon],$$
$$P_{gg}(z,\epsilon)=2N_C\left[\frac{z}{1-z}+\frac{1-z}{z}+z(1-z)\right],$$
$$P_{gq}(z,\epsilon)=C_F\left[\frac{1+(1-z)^2}{z}-\epsilon z\right],$$

and can be written

$$P_{ij}(z,\epsilon)=P_{ij}(z)+\epsilon P'_{ij}(z),$$

which defines the P'_{ij} functions. The functions F_{qq} and F_{qg} depend on the choice of factorization convention. The choice $\lambda=0$ is the universal convention while $\lambda=1$ is the physical convention. We adopt the physical convention and use

$$F_{qq}(z)=C_F\left[\frac{1+z^2}{1-z}\ln\left[\frac{1-z}{z}\right]-\frac{3}{2}\frac{1}{1-z}+2z+3\right],$$
$$F_{qg}(z)=[z^2+(1-z)^2]\ln\left[\frac{1-z}{z}\right]+8z(1-z)-1.$$

The functions F_{gg} and F_{gq} are not unambiguously determined in deep-inelastic scattering; we set them to zero, although other choices are possible.[18]

2. Three-body contributions

Since the three-body contribution to jet photoproduction is already of order $\alpha\alpha_s^2$ there are no corrections to consider. The cross section for this contribution is

$$\sigma_{3\text{ body}}(\gamma N\to\text{jets}+X)=\sum_{abcd}\int G_{b/N}(x_b,M^2)\times d\hat{\sigma}(\gamma b\to cde)dx_b.$$

The squared matrix elements for the $2\to3$ photoproduction subprocesses can be found in Refs. 16 and 17. The integration over three-body phase space and dx_b is done numerically by standard Monte Carlo techniques. The kinematic invariants s_{ij} and t_{ij} are first tested for soft and collinear singularities. If an invariant for a subprocess falls in a soft or collinear region of phase space, the contribution from that subprocess is not included in the cross section. Furthermore, if two final-state partons are separated in rapidity y and azimuthal angle ϕ by less than

$$\Delta R=\sqrt{(\Delta y)^2+(\Delta\phi)^2}<1,$$

the partons are coalesced and the event is classified as a two-jet event.

3. Photon-structure-function contributions

If events with beam jets are not vetoed, then contributions from the photon structure function must be included in the jet photoproduction calculation. This contribution is calculated by convoluting the $2\to2$ QCD subprocesses with the photon structure function and the proton structure function:

$$\sigma_{\text{PSF}}=\sum_{abcd}\int G_{a/\gamma}(x_a,M^2)G_{b/N}(x_b,M^2)\times\frac{d\hat{\sigma}}{dv}(ab\to cd)dx_a dx_b dv.$$

The squared matrix elements for the $2\to2$ QCD subprocesses can be found in Ref. 8.

The photon-structure-function contribution also has collinear corrections that are analogous to the collinear corrections for $\gamma q\to gq$ and $\gamma g\to q\bar{q}$. These corrections have the form

$$\frac{d\tilde{\sigma}}{dv}(ab\to cd)=\frac{d\hat{\sigma}}{dv}(ab\to cd)G_{b/N}(x_b,M^2)\frac{\alpha}{2\pi}\times\int_{x_a}^{1}\frac{dz}{z}G_{q/\gamma}(x_a,M^2)\times\left[P_{q\gamma}(z)\ln\left[\frac{1-z}{z}\delta_c\frac{s}{M^2}\right]-P'_{q\gamma}(z)-\lambda F_{q\gamma}(z)\right],$$

where a is q or $\bar{q}$ and b is q, $\bar{q}$, or g. The functions $P_{q\gamma}(z)$, $P'_{q\gamma}(z)$, and $F_{q\gamma}(z)$ are $6e_q^2$ times the respective functions $P_{qg}(z)$, $P'_{qg}(z)$, and $F_{qg}(z)$. The photon-structure-function contribution to jet photoproduction is then

$$\sigma_{\rm PSF}^{\rm NLL}(\gamma N\to\text{jets}+X)=\sum_{abcd}\int\left[G_{a/\gamma}(x_a,M^2)G_{b/N}(x_b,M^2)\frac{d\hat{\sigma}}{dv}(ab\to cd)+\frac{d\tilde{\sigma}}{dv}(ab\to cd)\right]dv\,dx_a dx_b\ .$$

[1]J. F. Owens, Phys. Rev. D **21**, 54 (1980).

[2]This nomenclature is borrowed from direct photon production where the time-reversed process $q\bar{q}\to\gamma g$ is referred to as the annihilation process.

[3]E. Witten, Nucl. Phys. **B120**, 189 (1977).

[4]R. J. DeWitt *et al.*, Phys. Rev. D **19**, 2046 (1979); **20**, 1751(E) (1979).

[5]Ch. Berger and W. Wagner, Phys. Rep. **146**, 1 (1987).

[6]M. Drees and R. M. Godbole, Phys. Rev. D **39**, 169 (1989); Phys. Rev. Lett. **61**, 682 (1988).

[7]H. Baer, J. Ohnemus, and J. F. Owens, Z. Phys. C **42**, 657 (1989).

[8]J. F. Owens, Rev. Mod. Phys. **59**, 465 (1987).

[9]L. Bergmann, Ph.D. dissertation, Report No. FSU-HEP-890215.

[10]L. Bergmann and J. F. Owens, Report No. FSU-HEP-890601 (unpublished).

[11]M. Drees and K. Grassie, Z. Phys. C **28**, 451 (1985).

[12]D. W. Duke and J. F. Owens, Phys. Rev. D **30**, 49 (1984).

[13]G. 't Hooft and M. Veltman, Nucl. Phys. **B44**, 189 (1972).

[14]W. A. Bardeen, A. J. Buras, D. W. Duke, and T. Muta, Phys. Rev. D **18**, 3998 (1978).

[15]G. Sterman and S. Weinberg, Phys. Rev. Lett. **39**, 1436 (1977).

[16]P. Aurenche, R. Baier, A. Douiri, M. Fontannaz, and D. Schiff, Nucl. Phys. **B286**, 553 (1987).

[17]The expressions in Ref. 16 for the $qq\to qq\gamma$ and $qq'\to qq'\gamma$ subprocesses contain a number of typographical errors where the variable a_3 appears in place of a_5. The original, Report No. LPTHE Orsay 86/24, contains the correct expressions.

[18]R. K. Ellis and J. C. Sexton, Nucl. Phys. **B269**, 445 (1986).